Title

PROPOSED MOLECULAR BEAM DETERMINATION OF ENERGY PARTITIOI IN THE PHOTODISSOCIATION OF POLYATOMIC MOLECULES

Authors

Zare, Richard N.
Herschbach, Dudley R.

Publication Date

1964-01-29

UCRL-11359

University of California

Ernest O. Lawrence Radiation Laboratory

PROPOSED MOLECULAR BEAM DETERMINATION OF ENERGY PARTITION IN THE PHOTODISSOCIATION OF POLYATOMIC MOLECULES

UCRL-11359
UC-4 Chemistry
TID-45 (27th Ed.)

UNIVERSITY OF CALIFORNIA

Lawrence Radiation Laboratory
Berkeley, California

AEC Contract No. W-7405-eng-48

PROPOSED MOLECULAR BEAM DETERMINATION OF ENERGY PARTITION IN THE PHOTODISSOCIATION OF POLYATOMIC MOLECULES

Richard N. Zare and Dudley R. Herschbach

January 29, 1964

UCRL-11359

PROPOSED MOLECULAR BEAM DETERMINATION OF ENERGY PARTITION IN THE PHOTODISSOCIATION OF POLYATOMIC MOLECULES*

Richard N. Zare[†‡] and Dudley R. Herschbach[‡]

Department of Chemistry and Lawrence Radiation Laboratory
University of California, Berkeley 4, California

Abstract

Conventional photochemical experiments give no information about the partitioning of energy between translational recoil and internal excitation of the fragment molecules formed in photodissociation of a polyatomic molecule. In a molecular beam experiment, it becomes possible to determine the energy partition from the form of the laboratory angular distribution of one of the photodissociation products. A general kinematic analysis is worked out in detail, and the uncertainty introduced by the finite angular resolution of the apparatus and the velocity spread in the parent beam is examined. The experimental requirements are evaluated for the photolysis of methyl iodide by the 2537 Å Hg line.

---

*Support received from the U. S. Atomic Energy Commission and the Alfred P. Sloan Foundation is gratefully acknowledged.

†National Science Foundation Predoctoral Fellow, 1961-64.

‡Present address: Department of Chemistry, Harvard University, Cambridge, Massachusetts, 02138.

Whenever a molecule is dissociated by absorbing radiation with a wavelength shorter than that required to rupture the chemical bond, the question arises as to the distribution of excess energy among the fragments. Often one or more of the dissociation products are formed in an excited electronic state, but in general there is additional excess energy which must appear in some other form. In the photodissociation of diatomic molecules, all energy above the dissociation threshold is transformed into kinetic energy of the recoiling atoms. However, for a polyatomic molecule the excess energy need not appear solely as translational energy, and may produce a high level of rotational or vibrational excitation of a molecular fragment.

It is evident that this initial partitioning of excess energy between translational and internal energy could play an important role in subsequent chemical reactions following photolysis. Quantitative measurement of the energy partition in the primary step of a photochemical reaction is not feasible in conventional experiments, however, due to the short lifetime of the reactive initial products and the rapid redistribution and thermalization of the excess energy through collisions.

This paper discusses the possibility of determining the initial energy partition by a molecular beam method, in which a collimated, collision-free stream of molecules is crossed with a beam of the exciting light. A kinematic analysis shows that the energy partition often can be measured solely from the form of the laboratory angular

distribution of one of the photodissociation products. The dependence of the distribution on the finite resolution of the detector and the velocity spread in the parent beam is examined for several different cases. The photolysis of methyl iodide by the mercury 2537 Å line is briefly studied as a prototype system.

Angular Distribution of Products

Consider a polyatomic molecule AB which on absorbing radiation of a known frequency dissociates into two parts,

$$AB \xrightarrow{h\nu} A + B \tag{1}$$

where A and B may be either atomic or molecular fragments. The absorption leading to dissociation is assumed to be an elementary process which occurs in a single vibration of the A—B bond. Let the energy E above the dissociation threshold of AB be partitioned into translational energy and internal energy,

$$E = E_T + E_I. \tag{2}$$

By conservation of linear momentum, the recoil velocities of A and B are given by

$$\underset{\sim}{v}_A = (2m_B E_T/mm_A)^{1/2} \tag{3a}$$

and

$$\underset{\sim}{v}_B = (2m_A E_T/mm_B)^{1/2} \tag{3b}$$

where m_A, m_B and m are respectively the masses of the A, B and AB molecules. If A refers to the heavier particle, the velocity of A

is less than that of B in the ratio of their masses,

$$|\underset{\sim}{v}_A| = (m_B/m_A)|\underset{\sim}{v}_B|. \qquad (4)$$

The angular distribution of the photodissociation products will be determined by the dependence of the transition probability on the relative orientation of the molecule and the electric vector of the light beam. The products separate rapidly enough to make negligible the blurring effect of the original rotational motion of the A—B molecule (except at the threshold for photodissociation).[1,2] Thus for an electric dipole excitation with a transition moment $\underset{\sim}{\mu}$, we may evaluate the angular distribution of products in the center of mass system simply by averaging $|\underset{\sim}{\mu}\cdot\underset{\sim}{\mathcal{E}}|^2$ over all rotational orientations of the molecule. In a previous treatment of the photodissociation of diatomic molecules[1], we have carried out this calculation in detail. Although the results are readily generalized, in order to clarify certain points we shall repeat some of the main steps here.

The average over rotational orientations is conveniently formulated in terms of the Eulerian angles ϕ, θ, ψ which relate a rotating "molecule-fixed" set of coordinate axes, xyz, to a nonrotating "space-fixed" system with axes parallel to specified laboratory directions, XYZ. For both systems the origin is the center-of-mass of the A—B molecule. The angles ϕ, θ are ordinary polar coordinates which locate the z axis relative to the Z axis and XY plane, and ψ is an azimuthal angle about the z axis. Since all orientations of the molecule are equally likely,

$$\sin\theta d\theta d\phi d\psi \tag{5}$$

is the (unnormalized) probability of an orientation with Eulerian angles in the range θ, ϕ, ψ to $\theta + d\theta$, $\phi + d\phi$, $\psi + d\psi$. If the electric vector has direction cosines λ_F along the space-fixed axes F = X,Y,Z and the transition dipole moment has direction cosines λ_g along the molecule-fixed axes g = x,y,z, the absorption probability is proportional to

$$|\underset{\sim}{\mu}\cdot\underset{\sim}{\mathcal{E}}|^2 = \mu^2\mathcal{E}^2|\sum_{Fg}\sum\lambda_F\lambda_g\Phi_{Fg}(\phi,\theta,\psi)|^2 \tag{6}$$

since $\mathcal{E}_F = \mathcal{E}\lambda_F$, $\mu_g = \mu\lambda_g$, and

$$\mu_F = \sum_g \Phi_{Fg}\mu_g,$$

where the angle dependent factors Φ_{Fg} are the direction cosines which describe the orthogonal transformation between the XYZ and xyz systems (see Table I). The probability that dissociation occurs for orientations in the range specified by (5) is thus given by

$$|\sum_{Fg}\sum\lambda_F\lambda_g\Phi_{Fg}(\phi,\theta,\psi)|^2\sin\theta d\theta d\phi d\psi. \tag{7}$$

We choose the z axis of the molecule-fixed system along the direction of departure of fragment A (opposite to that of B), so that the polar coordinates which describe the angular distribution of A in the center of mass system become identical to the Eulerian angles θ and ϕ. The intensity which enters the range θ, ϕ to $\theta + d\theta$, $\phi + d\phi$ is given by simply averaging (7) over ψ. By definition, this

intensity is

$$I(\theta,\phi)\sin\theta d\theta d\phi,$$

where $I(\theta,\phi)$ is the differential cross section per unit solid angle. Therefore we have

$$I(\theta,\phi) = \frac{1}{2\pi}\int_0^{2\pi} \left|\sum_{Fg}\lambda_F\lambda_g\Phi_{Fg}(\phi,\theta,\psi)\right|^2 d\psi. \qquad (8)$$

In most applications, including the various cases considered in reference 1, the cross products disappear and the general formula (8) reduces to the average of a single squared term,

$$I_{Fg}(\theta,\phi) = \frac{1}{2\pi}\int_0^{2\pi} \left|\Phi_{Fg}(\phi,\theta,\psi)\right|^2 d\psi, \qquad (9)$$

or to a sum of such terms. The FF' cross products disappear if one of the axes, say the Z-axis, is chosen to lie along the electric vector for the case of plane-polarized light, or along the direction of the light beam, for unpolarized light. In the latter case, the $\mathcal{E}_X$ and $\mathcal{E}_Y$ components of the electric vector are equal in magnitude but contribute independently as they represent the resultant amplitude of many plane-polarized waves with random phases. The gg' cross products also disappear for diatomic molecules and for many transitions in symmetrical polyatomic molecules for which the transition dipole moment $\underset{\sim}{\mu}$ is either parallel or perpendicular to the A—B axis. Although the transition which induces photodissociation may have several components, of both the parallel and perpendicular type, again these contribute independently.

Table I gives the direction cosine elements[3,4] Φ_{Fg} which appear

in (8) and their azimuthally averaged squares I_{Fg} which appear in (9). From these formulas angular distributions are readily evaluated for any type of electric dipole transition. It should be noted that Table I differs from Table III of reference 1 in that ϕ and ψ in the latter are replaced by $\phi + \frac{\pi}{2}$ and $\frac{\pi}{2} - \psi$, respectively. This change does not affect any of the calculations of reference 1, but is necessary to make the Eulerian angles θ and ϕ correspond to ordinary polar coordinates. (Compare the discussion on p.7, reference 4, with that on p. 108, reference 3.)

Table II gives the angular distributions for the case of independent parallel and perpendicular transitions. The more general case will not be examined here, as at present we are primarily interested in simple molecules, such as CH_3I, for which this classification is adequate. As indicated in Table II, the direction of the Z-axis has been chosen to bring out the symmetry of the distributions, and this makes them independent of the angle ϕ. The cross sections peak at right angles to the incident light beam for a parallel transition and peak forward and backward for a perpendicular transition.

In the kinematic analysis of the molecular beam experiment which is carried out in later sections of this paper, it is most convenient to put the Z-axis along the direction of the molecular beam. The cross section formulas for this reference system are given in Table III for various choices of the experimental geometry. The direction labelled "preferred recoil" is the direction in which the angular distribution

peaks in the center of mass system. The kinematic analysis shows that the optimum arrangement should put the preferred direction of recoil in the center of mass system transverse to the direction of the molecular beam, in order to make the laboratory angular distribution as sensitive as possible to the way the energy is partitioned. In Table III the experimental arrangements which correspond to this are marked with an asterisk, and Figure 1 shows sections of these distributions in the XY, YZ, and XZ planes for a set-up in which the light beam is incident along the X axis and the molecular beam along the Z axis.

In Table III the FF' cross products in (8) are absent because the electric vector, or the direction of the light beam in the unpolarized case, is chosen to lie along one of the coordinate axes. However, there is some advantage in varying the orientation of the electric vector and thereby shifting the direction in which the differential cross section peaks, as this offers a check on the kinematic analysis of the angular distribution. Thus we will briefly consider the formulas applicable to this case. Without loss of generality we may suppose the electric vector is aimed in the direction $\theta = \Theta$ in the YZ plane. Then in (8) we have $\lambda_X = 0$, $\lambda_Y = \sin\Theta$, and $\lambda_Z = \cos\Theta$, and the integration yields

$$I_{||}(\theta,\phi) = S^2\phi S^2\theta S^2\Theta + 2S\phi S\theta C\theta S\Theta C\Theta + C^2\theta C^2\Theta \qquad (10a)$$

and

$$I_{\perp}(\theta,\phi) = (C^2\phi + S^2\phi C^2\theta)S^2\Theta - S\phi S\theta C\theta S\Theta C\Theta + S^2\theta C^2\Theta \qquad (10b)$$

for parallel (g = z) and perpendicular (g = x) transitions, respectively. As before, S denotes sine and C denotes cosine. Formula (10a) should be

Table I. Transformation coefficients in terms of Eulerian angles.

Direction of Transition Dipole	Direction of Electric Field F = X	Y	Z
	Direction cosine factors, Φ_{Fg}		
g = x	$-S\phi S\psi - C\phi C\theta C\psi$	$C\phi S\psi - S\phi C\theta C\psi$	$S\theta C\psi$
y	$S\phi C\psi - C\phi C\theta S\psi$	$-C\phi C\psi - S\phi C\theta S\psi$	$S\theta S\psi$
z	$C\phi S\theta$	$S\phi S\theta$	$C\theta$
	Azimuthally averaged squares, I_{Fg}		
x or y	$\frac{1}{2}(S^2\phi + C^2\phi C^2\theta)$	$\frac{1}{2}(C^2\phi + S^2\phi C^2\theta)$	$\frac{1}{2}S^2\theta$
z	$C^2\phi S^2\theta$	$S^2\phi S^2\theta$	$C^2\theta$

Here sine is abbreviated by S, cosine by C.

Table II. Differential cross section $I(\theta)$ in center-of-mass system.

Electronic Transition	$I(\theta)$
For polarized light with electric vector along Z-axis	
$\parallel$	$3\cos^2\theta = 1+2P_2$
$\perp$	$\frac{3}{2}\sin^2\theta = 1-P_2$
For unpolarized light incident along Z-axis	
$\parallel$	$\frac{3}{2}\sin^2\theta = 1-P_2$
$\perp$	$\frac{3}{4}(1+\cos^2\theta) = 1+\frac{1}{2}P_2$

where

$$P_2 = \frac{1}{2}(3\cos^2\theta-1)$$

$$\int_0^{2\pi}\int_0^{\pi} I(\theta)\sin\theta d\theta d\phi = 4\pi$$

Table III. Differential cross section in center of mass system for various choices of crossed beam geometry.

Electronic Transition	Special Directions			Cross Section $I(\theta,\phi)$
	Light Beam	Electric Vector	Preferred Recoil	
	For polarized light			
$\parallel$	X or Y	Z	Z	$3\cos^2\theta$
$\parallel$	X or Z	Y	Y*	$3\sin^2\theta\sin^2\phi$
$\perp$	X or Y	Z	X or Y*	$\frac{3}{2}\sin^2\theta$
$\perp$	X or Z	Y	X* or Z	$\frac{3}{2}(1-\sin^2\theta\sin^2\phi)$
	For unpolarized light			
$\parallel$	Z		X or Y*	$\frac{3}{2}\sin^2\theta$
$\parallel$	X		Y* or Z	$\frac{3}{2}(1-\sin^2\theta\cos^2\phi)$
$\perp$	Z		Z	$\frac{3}{4}(1+\cos^2\theta)$
$\perp$	X		X*	$\frac{3}{4}(1+\sin^2\theta\cos^2\phi)$

The Z-axis is along the molecular beam direction and the cross sections are normalized to 4π.

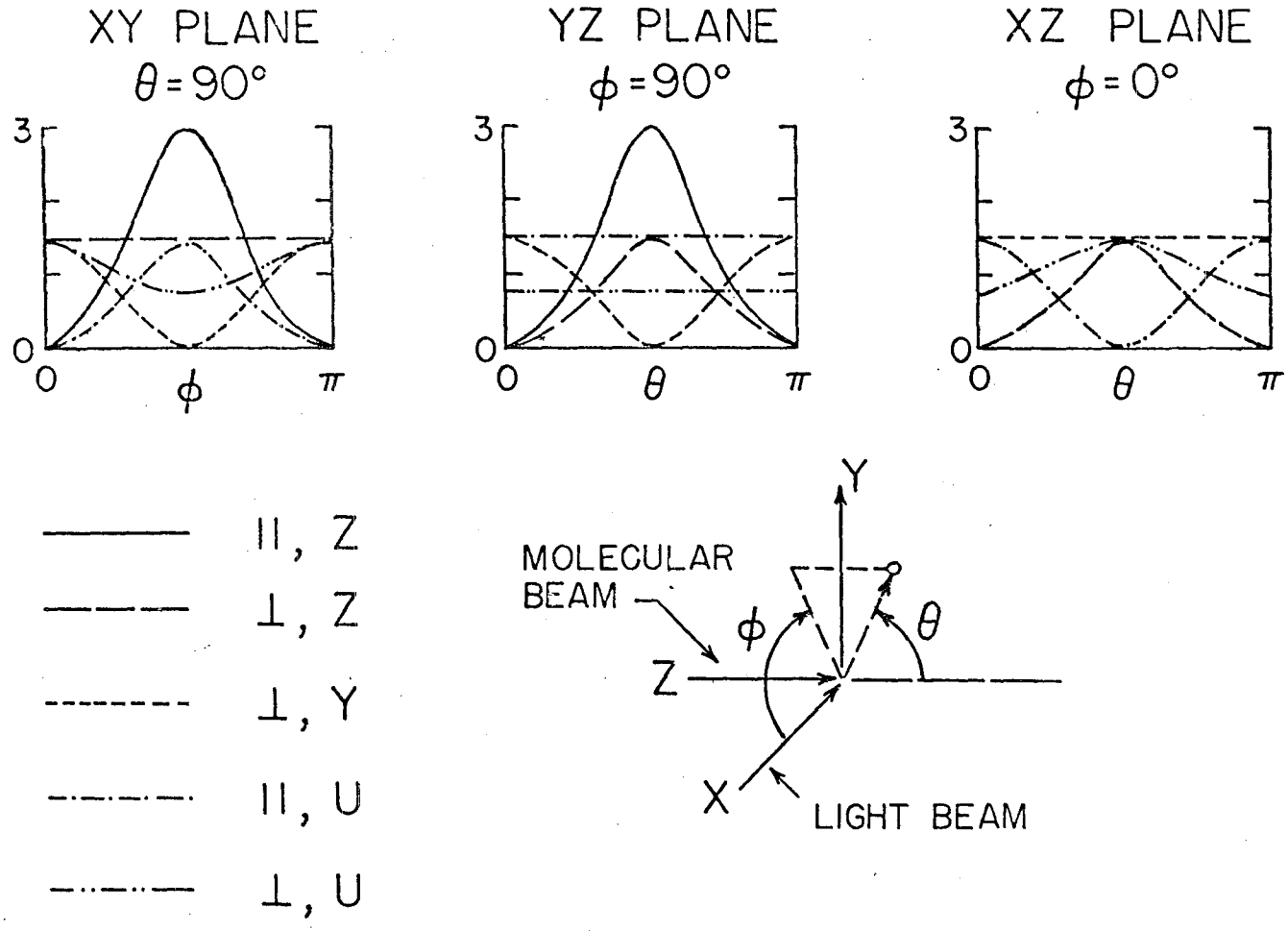

Fig. 1. Sections of the angular distributions in the center of mass system for parallel (||) or perpendicular (⊥) transitions and plane polarized (along Z or Y axis) or unpolarized (U) exciting light. The light beam is incident along the X axis and the molecular beam along the Z axis.

multiplied by a factor of 3 and (10b) by a factor of 3/2, to normalize the results to 4π. In the YZ plane, where $\phi = 90°$, the normalized formulas reduce to

$$I_{||}(\theta,\tfrac{\pi}{2}) = 3\cos^2(\theta-\Theta) \qquad (11a)$$

and

$$I_{\perp}(\theta,\tfrac{\pi}{2}) = \tfrac{3}{2}\sin^2(\theta-\Theta), \qquad (11b)$$

as would be expected from the results of Table II.

Kinematic Relations

In collisions of thermal molecules with light quanta, practically all the linear momentum is carried by the molecule. For example, the most probably translational momentum of a beam of CH_3I molecules at 300°K is 4×10^{-18} cgs/molecule, whereas for light of wavelength 2537 Å the momentum is only 4×10^{-22} cgs/photon, smaller by a factor of 10^4. When photodissociation occurs, the center of mass of the fragments travels along the original direction of the parent molecular beam with its original momentum. Since the laboratory velocity of a fragment molecule is the vector resultant of its recoil velocity and the velocity of the parent molecular beam, the angular distribution of the products in the laboratory is skewed towards the forward direction of the beam.

The extent of this forward displacement depends on the form of the angular distribution of recoil vectors which, for electric dipole transitions, is calculable from (8) or (9), and on the ratio,

$$x = |\underset{\sim}{V}|/|\underset{\sim}{v}|, \tag{12}$$

of the velocity $\underset{\sim}{V}$ of the parent molecular beam to the recoil velocity $\underset{\sim}{v}$ of the observed fragment molecule. Thus if the shape of the angular distribution observed in the laboratory proves to be sufficiently sensitive to the kinematic parameter x, it will provide a measure of the recoil velocity and the energy partitioning may be determined from Eqs. (2) and (3).

Many discussions of scattering kinematics and the transformation between the center of mass and laboratory coordinate systems are available.[5,6] However, the sugject is seldom considered in detail and there appears to be no explicit treatment of several important features. Accordingly, it seems worthwhile to give a rather detailed treatment here.

All of the kinematic relationships follow from the velocity vector diagrams of Fig. 2, where

θ_o = laboratory angle at which product fragment is observed

θ = corresponding angle of recoil of the fragment in a coordinate system traveling with the center of mass (that is, with the parent molecular beam)

$\underset{\sim}{V}$ = velocity of the center of mass in the laboratory = velocity of the molecular beam

$\underset{\sim}{v}_o$ = velocity of fragment in the laboratory coordinate system

$\underset{\sim}{v}$ = recoil velocity of fragment in the center of mass coordinate system.

The angles θ, ϕ in the center of mass (CM) system are related to the

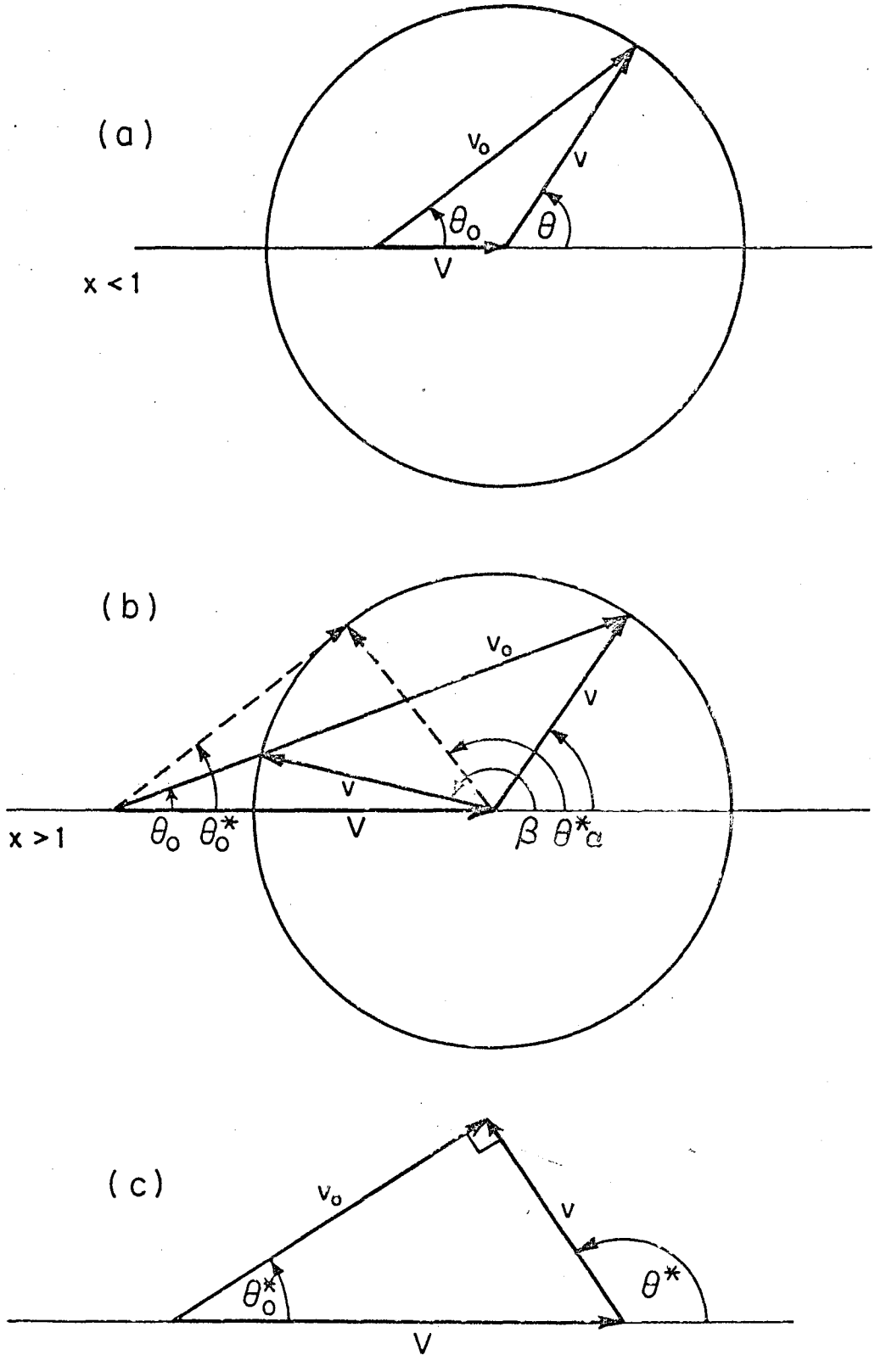

Fig. 2. Velocity vector diagrams relating the center of mass and laboratory systems (a) for $x < 1$, (b) for $x > 1$, and (c) for the "edge effect" on the "singular sphere".

laboratory (LAB) angles θ_o, ϕ_o by

$$v\cos\theta + V = v_o\cos\theta_o \tag{13a}$$

$$v\sin\theta = v_o\sin\theta_o \tag{13b}$$

$$\phi = \phi_o \tag{13c}$$

Making use of the law of cosines,

$$v_o^2 = V^2 + v^2 + 2vV\cos\theta,$$

we may express θ_o in terms of θ in several ways:

$$\tan\theta_o = \frac{\sin\theta}{\cos\theta + x} \tag{14a}$$

$$\sin\theta_o = \frac{\sin\theta}{\sqrt{1 + 2x\cos\theta + x^2}} \tag{14b}$$

and

$$\cos\theta_o = \frac{\cos\theta + x}{\sqrt{1 + 2x\cos\theta + x^2}} . \tag{14c}$$

The inverse transformation can be readily obtained from Eq. (14c) by squaring and rearranging it to yield a quadratic expression,

$$\cos^2\theta + 2x\sin^2\theta_o\cos\theta + x^2\sin^2\theta_o - \cos^2\theta_o = 0,$$

which has the roots

$$\cos\theta = -x\sin^2\theta_o \pm \cos\theta_o \sqrt{1 - x^2\sin^2\theta_o}. \tag{15}$$

Hence the transformation between the laboratory angles θ_o, ϕ_o and the center of mass angles θ, ϕ is completely specified in terms of x by Eqs. (14) and (15).

For $x < 1$ the relation between θ and θ_o is one to one, as can be seen from Fig. 2a. As θ varies from 0 to π, the angle θ_o varies

between the same limits. The plus sign must be taken in Eq. (15) so that $\theta = 0$ when $\theta_o = 0$.

For $x > 1$, however, the relation is double-valued. For each value of θ_o there are two values of θ, corresponding to the two different signs in (15). For the value of θ_o shown in Fig. 2b there are two values of θ, denoted by α and β, that are determined by the forward and backward recoil vectors v which correspond to the same laboratory vector v_o. As θ varies from 0 to π, the laboratory angle θ_o increases until it reaches a maximum value θ_o^* corresponding to θ^*, and then θ_o decreases to zero again. Thus we distinguish two branches,

$$\theta = \alpha: \quad 0 \leq \alpha \leq \theta^*, \quad 0 \leq \theta_o \leq \theta_o^*$$

$$\theta = \beta: \quad \theta^* \leq \beta \leq \pi, \quad \theta_o^* \geq \theta_o \geq$$

The relationship between these branches is readily obtained from Fig. 2b; since the α and β recoil vectors define an isosceles triangle,

$$\pi - (\beta - \theta_o) = \alpha - \theta_o$$

or

$$\beta = \pi - \alpha + 2\theta_o. \tag{16}$$

The transformation for the β branch thus can be expressed in terms of that for the α branch, with proper allowance for the fact that β decreases as α increases. When $\alpha = \beta = \theta^*$, the laboratory angle reaches its maximum θ_o^*, and from (16) we find

$$\theta^* = \theta_o^* + \frac{\pi}{2}. \tag{17}$$

As pictured in Fig. 2c, this relation means that the recoil velocity

vector v is at right angles to the laboratory velocity v_o. Also, we see that the critical angle is simply related to the kinematic parameter (12), as

$$\frac{1}{x} = \sin\theta_o^* . \tag{18}$$

The analysis of angular distributions requires a transformation of the differential solid angle elements in the CM and LAB systems,

$$d\omega = \sin\theta d\theta d\phi \text{ and } d\omega_o = \sin\theta_o d\theta_o d\phi_o .$$

By differentiating both sides of (14c), we obtain the Jacobian factor,

$$J(x,\theta) = d\omega/d\omega_o = \frac{(1 + 2x\cos\theta + x^2)^{3/2}}{|1 + x\cos\theta|} , \tag{19a}$$

Similarly, by differentiating (15) we obtain the inverse Jacobian,

$$J_o(x,\theta_o) = d\omega_o/d\omega = \left[2x\cos\theta_o \pm \frac{1 + x^2\cos 2\theta_o}{\sqrt{1 - x^2\sin^2\theta_o}}\right]^{-1} , \tag{19b}$$

where the plus sign is taken for $x < 1$. For $x > 1$, the plus sign is taken for the α branch, the minus sign for the β branch.

The total number of particles emitted into corresponding solid angle elements must be the same in the CM and LAB systems, and therefore the differential cross sections are related by

$$I(\theta_o,\phi_o)d\omega_o = I(\theta,\phi)d\omega. \tag{20}$$

Accordingly, the transformation of angular distributions is given by

$$I(\theta_o,\phi_o) = J(x,\theta)I(\theta,\phi) \tag{21a}$$

and

$$I(\theta,\phi) = J_o(\kappa,\theta_o)I(\theta_o,\phi_o). \tag{21b}$$

Note that since $\phi = \phi_o$, each cone θ = constant in the CM system is transformed into a cone θ_o = constant in the LAB system. In particular, for $\theta = 90°$,

$$\theta_o = \arctan(1/\kappa) < 90° \tag{22a}$$

and

$$I(\theta_o,\phi_o) = (1+\kappa^2)^{3/2} I(\theta,\phi). \tag{22b}$$

Likewise, if $\kappa < 1$, observations on the $\theta_o = 90°$ plane in the LAB system correspond in the CM system to

$$\theta = \arccos(-\kappa) > 90° \tag{23a}$$

and

$$I(\theta,\phi) = (1-\kappa^2)^{-\frac{1}{2}} I(\theta_o,\phi_o). \tag{23b}$$

In principal these relations, together with the freedom of adjustment of the CM angular distribution provided by (11), offer a means to determine both the angular dependence of the photodissociation probability and the energy partitoning.

Sample Calculations of Laboratory Angular Distributions

From Fig. 1 and Table III it is seen that, for transitions which give angular distributions in the CM system which peak at right angles to the beam direction, only the three types of θ-dependence indicated in Table IV need to be considered. Also, since (23) accounts for the

distribution in the XY plane of the CM system, we may restrict attention to the XZ and YZ planes.

The variation of the form of the laboratory angular distribution with the kinematic parameter x is illustrated in Figs. 3 - 8 for transitions of the three types A, B, and C. The transformation (21b) was carried out by an IBM 7090 computer program and Figs. 3 - 8 prepared directly from the computer output via a XY digital incremental plotter.

For $x = 0$, when the velocity of the parent molecular beam is negligible in comparison with the recoil velocity of the fragment molecule, the LAB and CM angular distributions are identical. For $x < 1$, since the recoil is "fast" relative to the beam velocity, the LAB distribution preserves the main features of the CM distribution. As $x \to 1$, it is strongly skewed toward the forward direction of the beam, and at $x = 1$, for which $\theta_o = \frac{1}{2}\theta$, no particles can appear in the backward hemisphere of the laboratory distribution.

For $x > 1$, the recoil is "slow" compared with the parent beam velocity, and the product fragments are confined to a forward cone of half angle $\theta_o^* = \arcsin(1/x)$. Outside this cone ($\theta_o > \theta_o^*$) there is no intensity, and within it ($\theta_o < \theta_o^*$) both the α and β branches of the CM distribution contribute at each laboratory angle θ_o. For x larger than 2 or 3, the CM angular distribution is compressed into such a small range of laboratory angles (see Figs. 9-11) that very little can be deduced about the form of $I(\theta,\phi)$, especially in cases

Table IV. Classification of angular dependence of cross sections.

Type of Transition	Dependence on θ	Definition of Conditions Obs. Plane	Sym.	Light
A	$\sin^2\theta$	YZ	$\parallel$	$\mathcal{E}_Y$
		YZ	$\perp$	$\mathcal{E}_Z$
		XZ or YZ	$\parallel$	U_Z
B	$1 + \sin^2\theta$	XZ	$\perp$	U_X
C	none	YZ	$\parallel$	U_X
		XZ	$\perp$	$\mathcal{E}_Y$
		YZ	$\perp$	U_X

The Z-axis is along the molecular beam direction. The nature of the light beam is indicated by $\mathcal{E}_F$, if it is plane-polarized with the electric vector along the F-axis, or by U_F, if it is unpolarized and travelling along the F-axis.

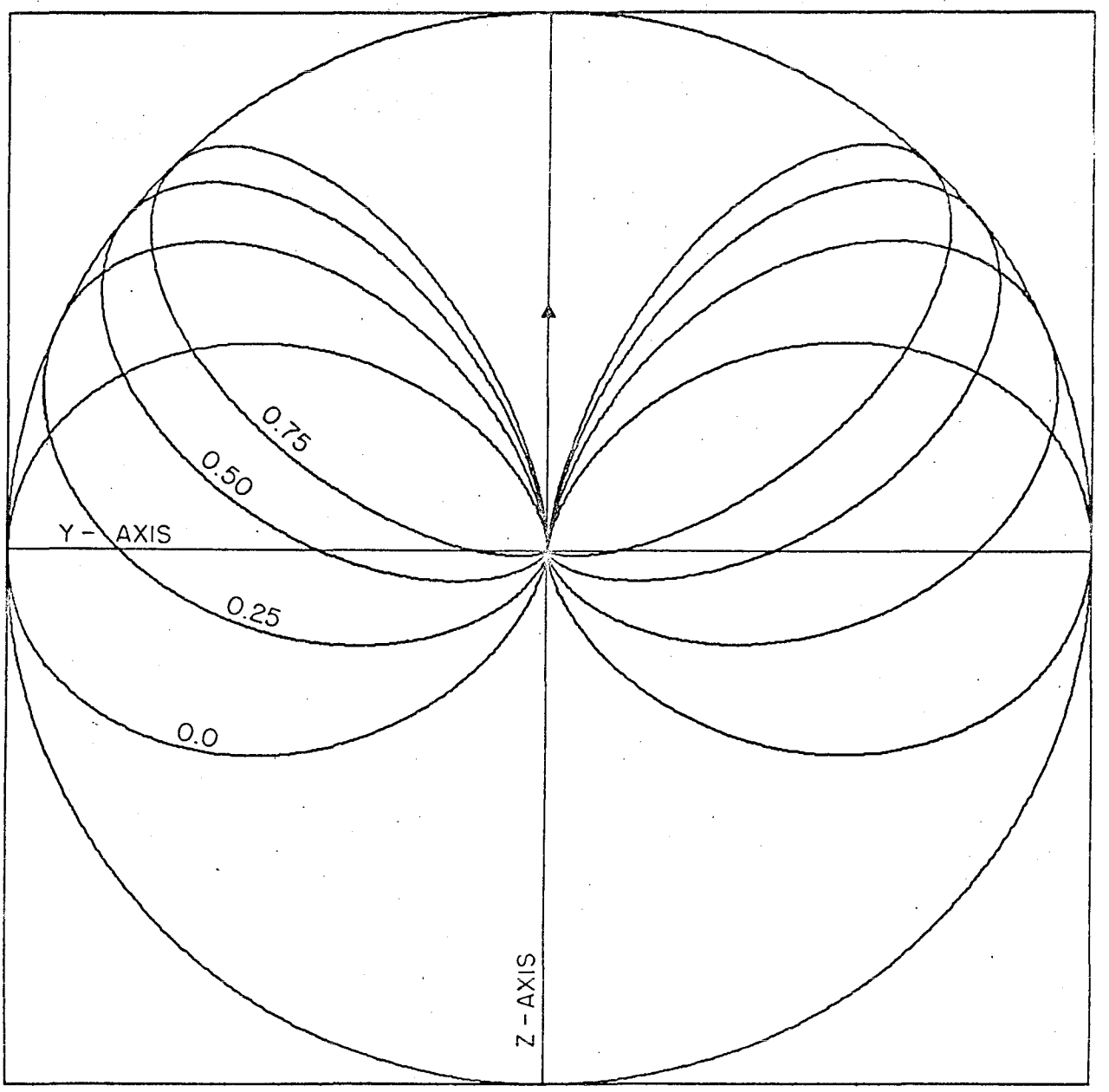

Fig. 3. Polar plot of laboratory differential cross sections in the YZ plane for a type A transition and various values of $x < 1$, corresponding to "fast recoil". All plots shown have been scaled to unit radius. To preserve normalization among these cross-sections, the plot for $x = 0.25$ must be multiplied by 1.146, the plot for $x = 0.50$ by 1.531 and the plot for $x = 0.75$ by 2.129.

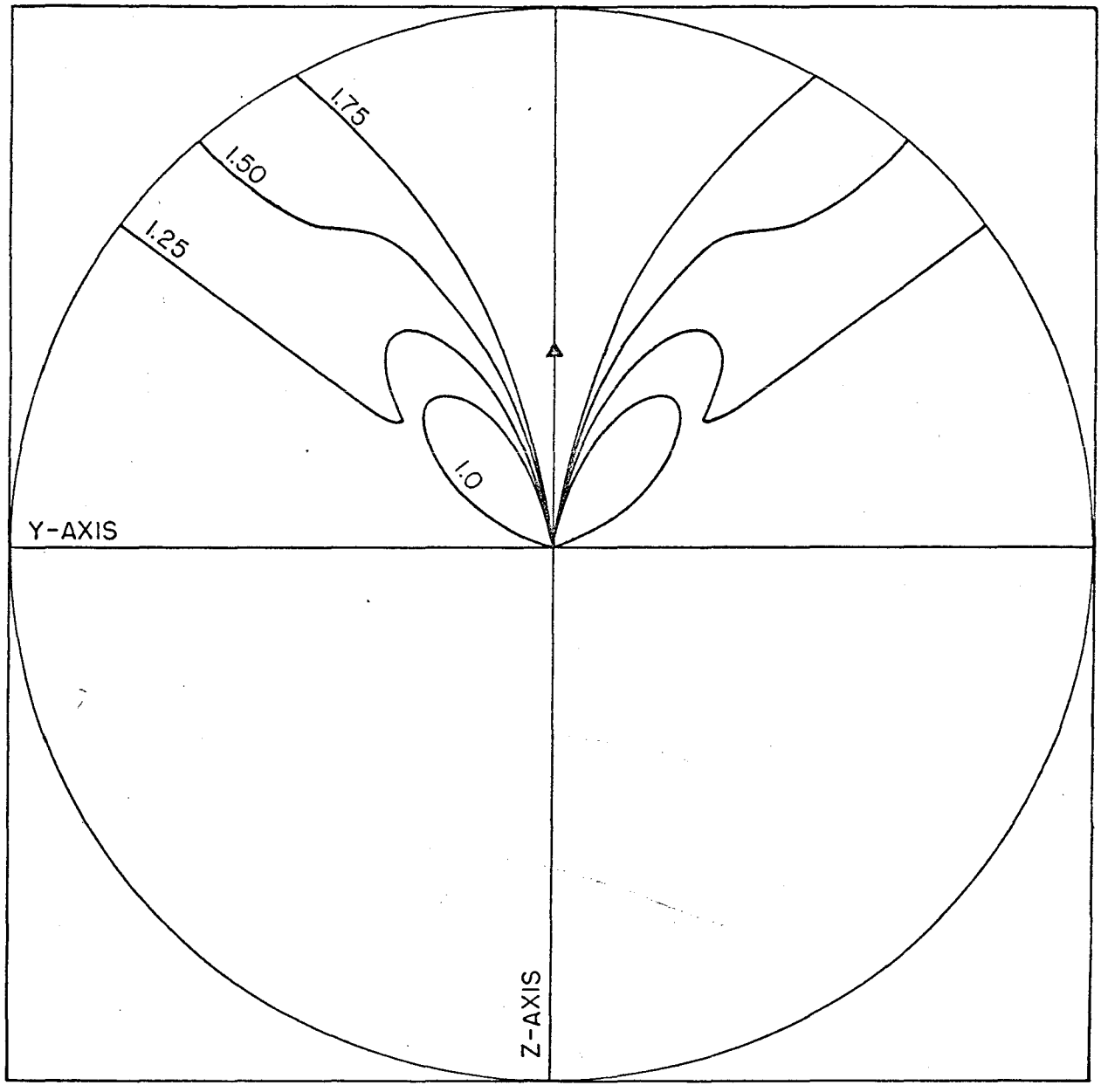

Fig. 4. Polar plot for laboratory differential cross section in the YZ plane for a type A transition and various values of $x \geq 1$, corresponding to "slow recoil". If the circle is taken as unit radius, all plots must be multiplied by 2.5 to be normalized to 4π.

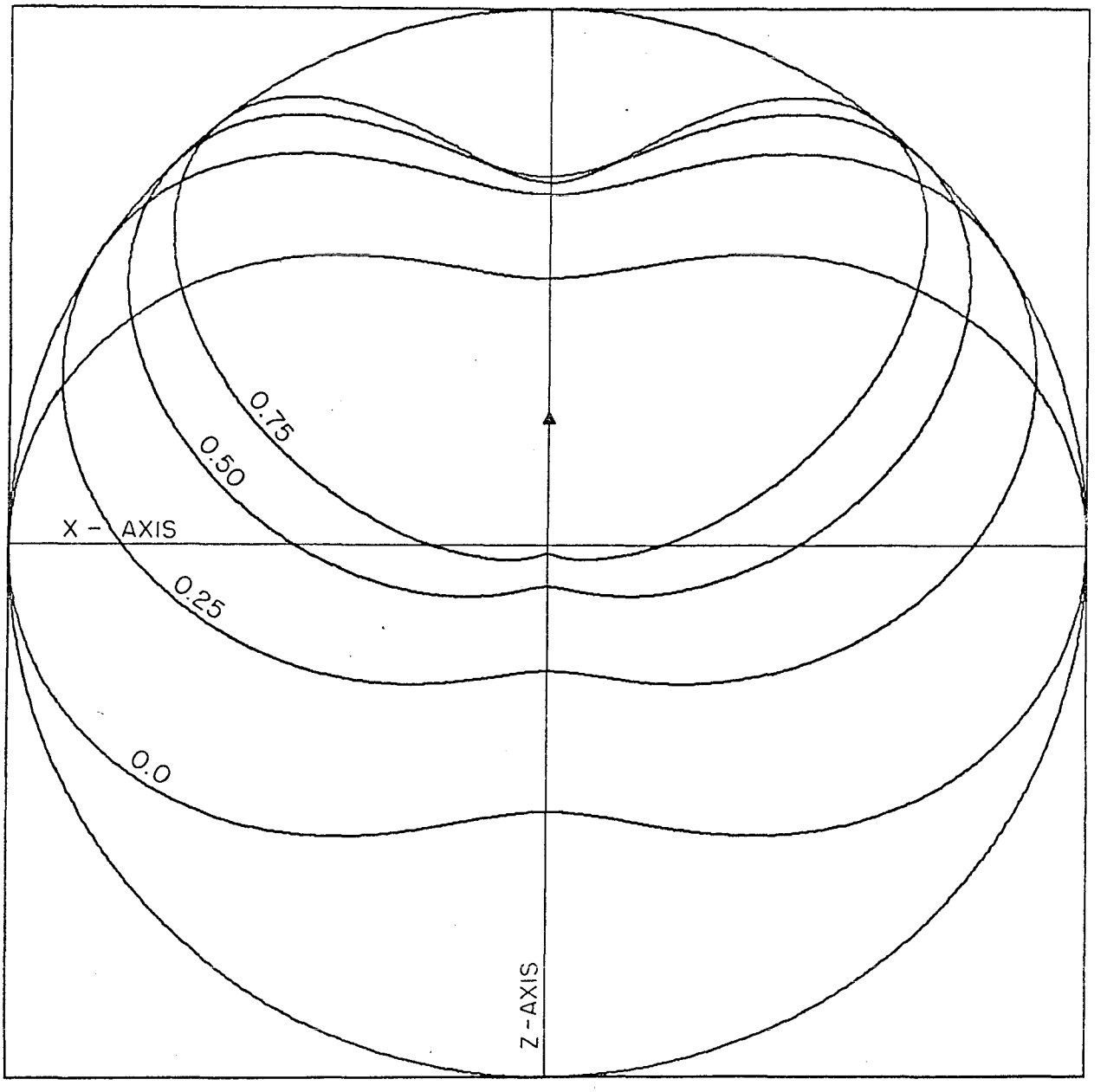

Fig. 5. Polar plot of laboratory differential cross section in the XZ plane for a type B transition and various values of $x < 1$, corresponding to "fast recoil". All plots shown have been scaled to unit radius. To preserve normalization among these cross-sections, the plot for $x = 0.25$ must be multiplied by 1.265, the plot for $x = 0.50$ by 2.346 and the plot for $x = 0.75$ by 3.730.

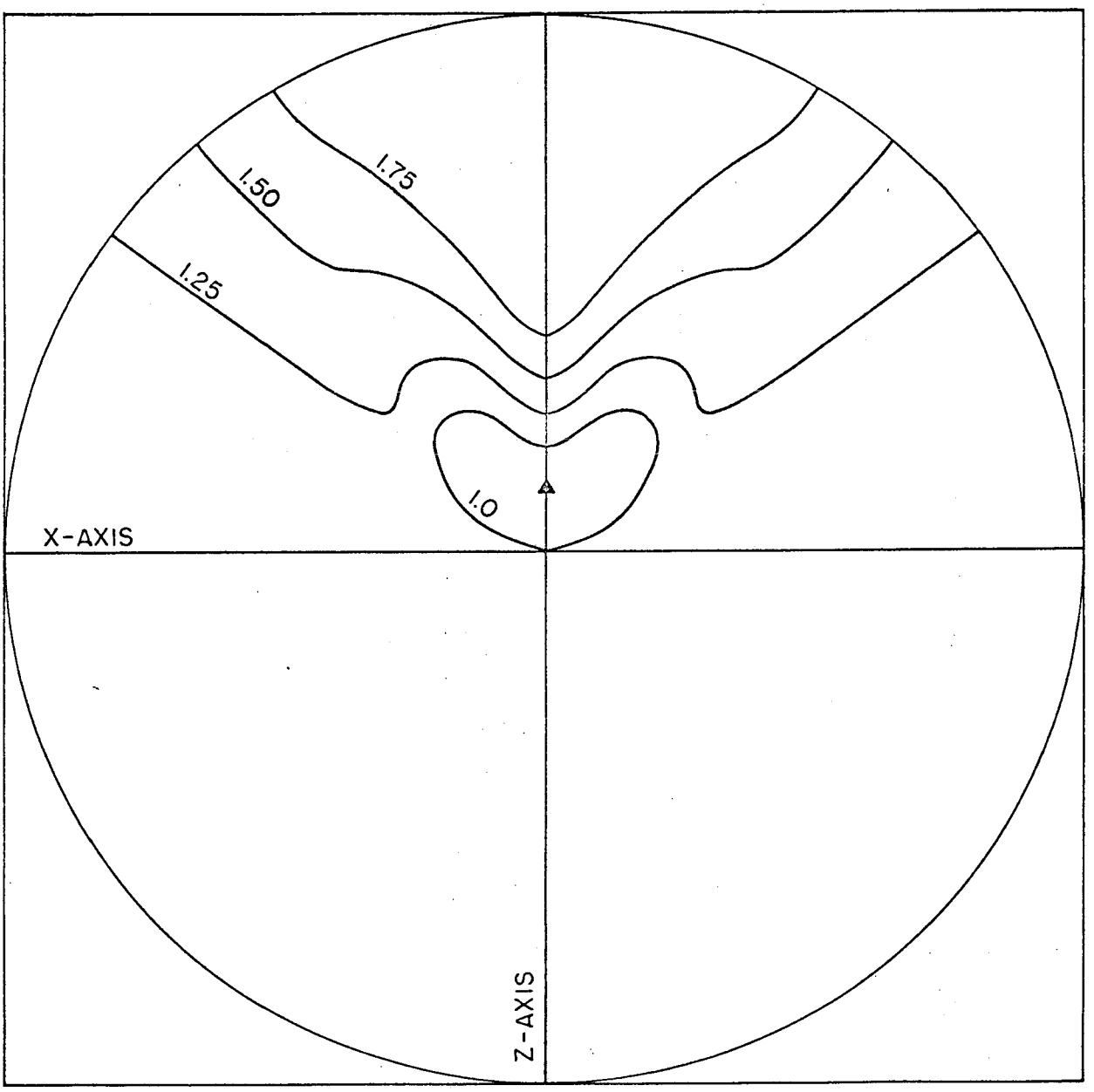

Fig. 6. Polar plot of laboratory differential cross section in the XZ plane for a type B transition and various values of $x \geq 1$, corresponding to "slow recoil". If the circle is taken as unit radius, all plots must be multiplied by 3.0 to be normalized to 4π.

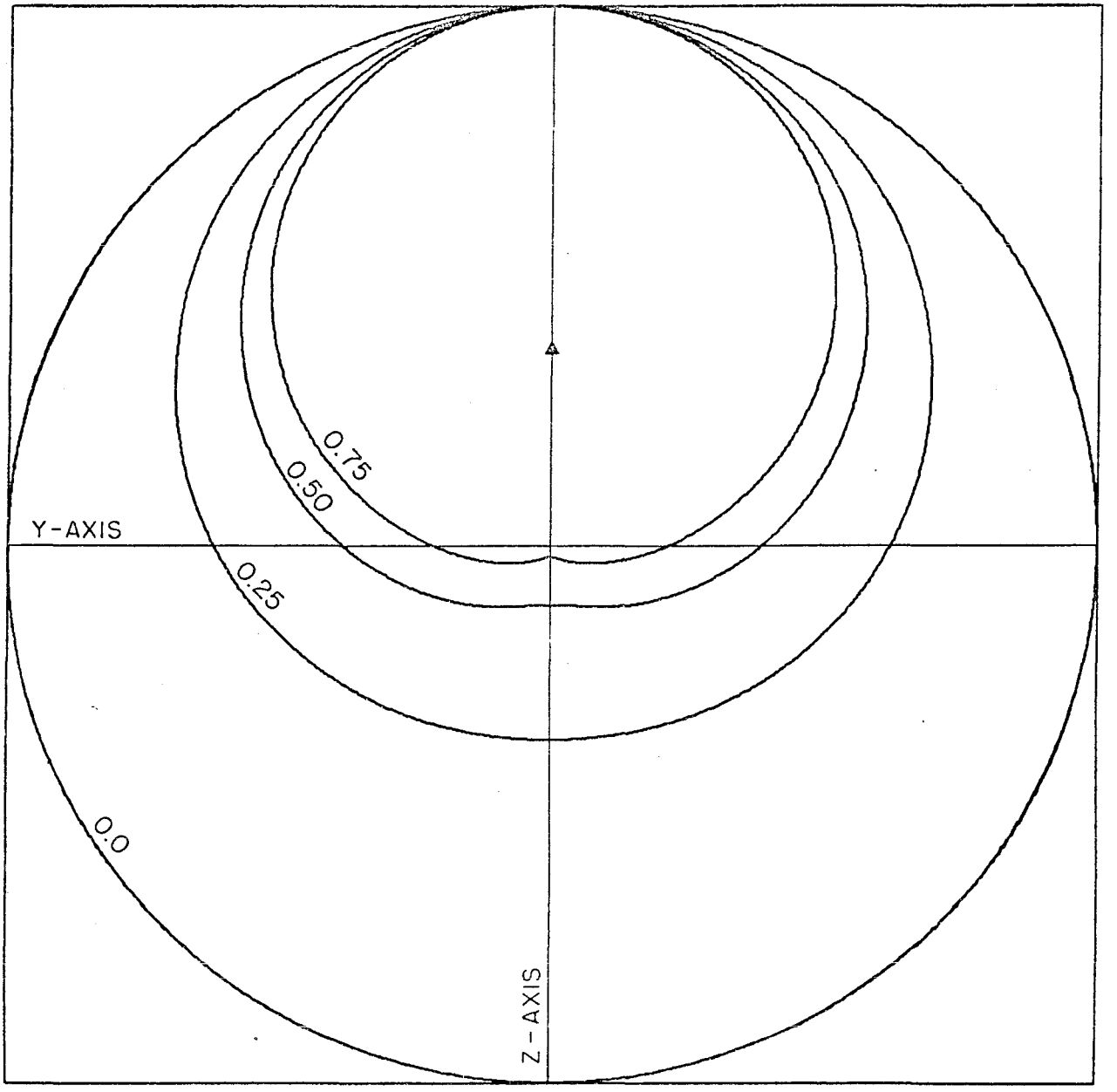

Fig. 7. Polar plot of laboratory differential cross section in the XZ or YZ planes for a type C transition and various values of $x < 1$, corresponding to "fast recoil". All plots shown have been scaled to unit radius. To preserve normalization among these cross-sections, the plot for $x = 0.25$ must be multiplied by 1.384, the plot for $x = 0.50$ by 2.472 and the plot for $x = 0.75$ by 4.396.

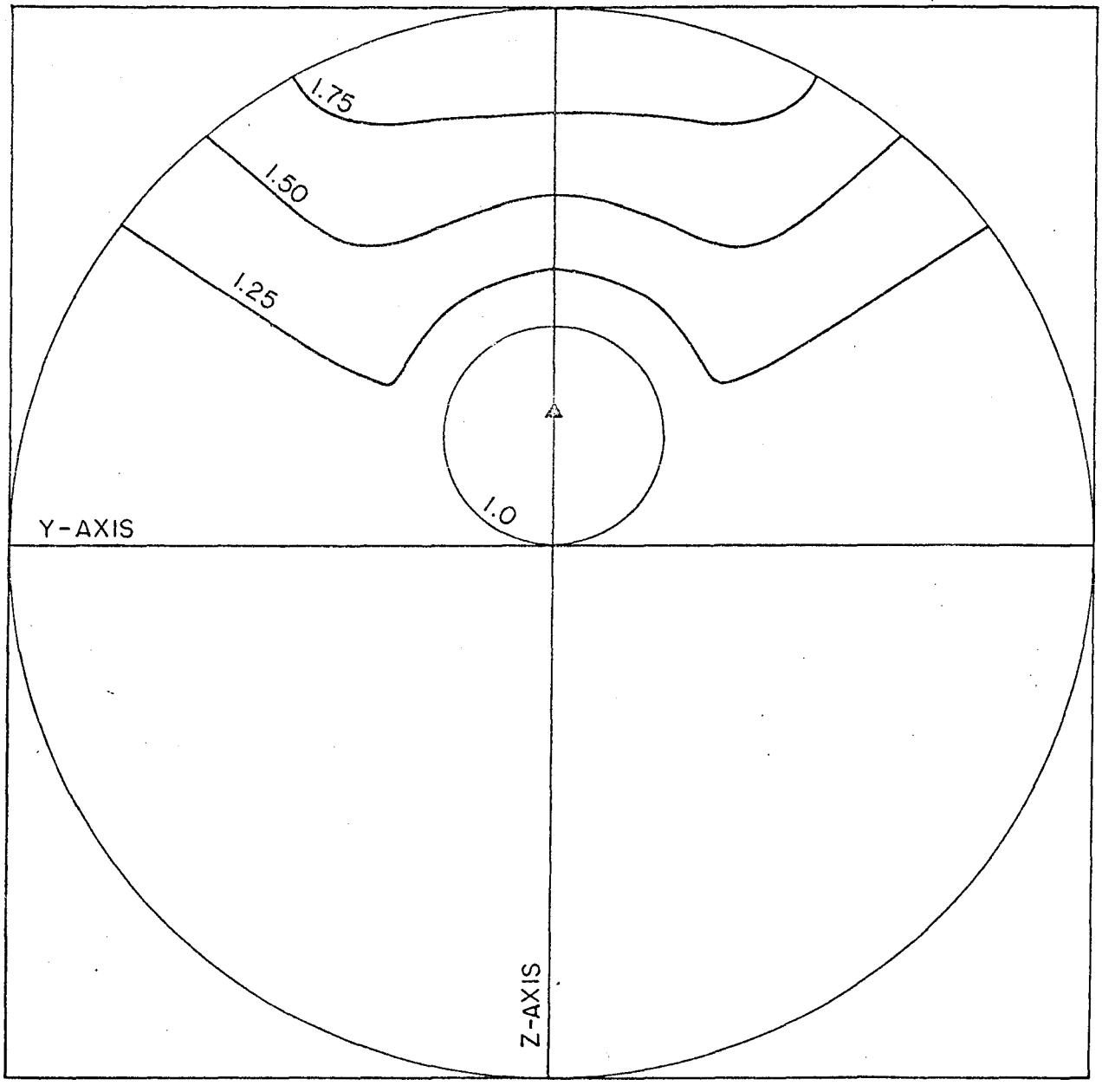

Fig. 8. Polar plot of laboratory differential cross section in the XZ or YZ planes for a type C transition and various values of $x \geq 1$, corresponding to "slow recoil". All plots are normalized to 4π, if the circle is taken as unit radius.

for which the α and β branches both give important contributions.

The "Edge Effect" and the "Singular Sphere"

Another special feature arises for the case of slow recoil ($x > 1$). As the edge of the forward cone is approached ($\theta_o \to \theta_o^*$), the laboratory solid angle element becomes vanishingly small ($d\omega_o \to 0$), as may be seen from (17)-(19) and in Figs. 2c and 9, and the Jacobian factor $J(x,\theta)$ in (21a) becomes infinite. Near the singular point, $\theta = \theta^* + \delta\theta$, the transformation relations may be expanded, and

$$J(x,\theta) \approx \frac{x^2 - 1}{\delta\theta} + \ldots \tag{24a}$$

$$I(\theta,\phi) \approx I(\theta^*,\phi) + I'(\theta^*,\phi)\delta\theta + \ldots \tag{24b}$$

or

$$I(\theta_o,\phi_o) \approx (x^2 - 1)\,\frac{I(\theta^*,\phi)}{\delta\theta} + \ldots \tag{24c}$$

Thus, unless the CM angular distribution becomes vanishingly small as $\theta \to \theta^*$, the LAB distribution will exhibit a singularity as $\theta_o \to \theta_o^*$. Examples appear in Figs. 4, 6, 8 and 9. We refer to this as the "edge effect", since it arises because at $\theta_o = \theta_o^*$ the laboratory observer is viewing the CM angular distribution "edge on".

As this situation occurs whenever the LAB and CM velocity vectors are perpendicular, as pictured in Fig. 2c, the locus of all such recoil vectors defines a "singular sphere" with the beam velocity V as a diameter. How much of this sphere is accessible depends solely on

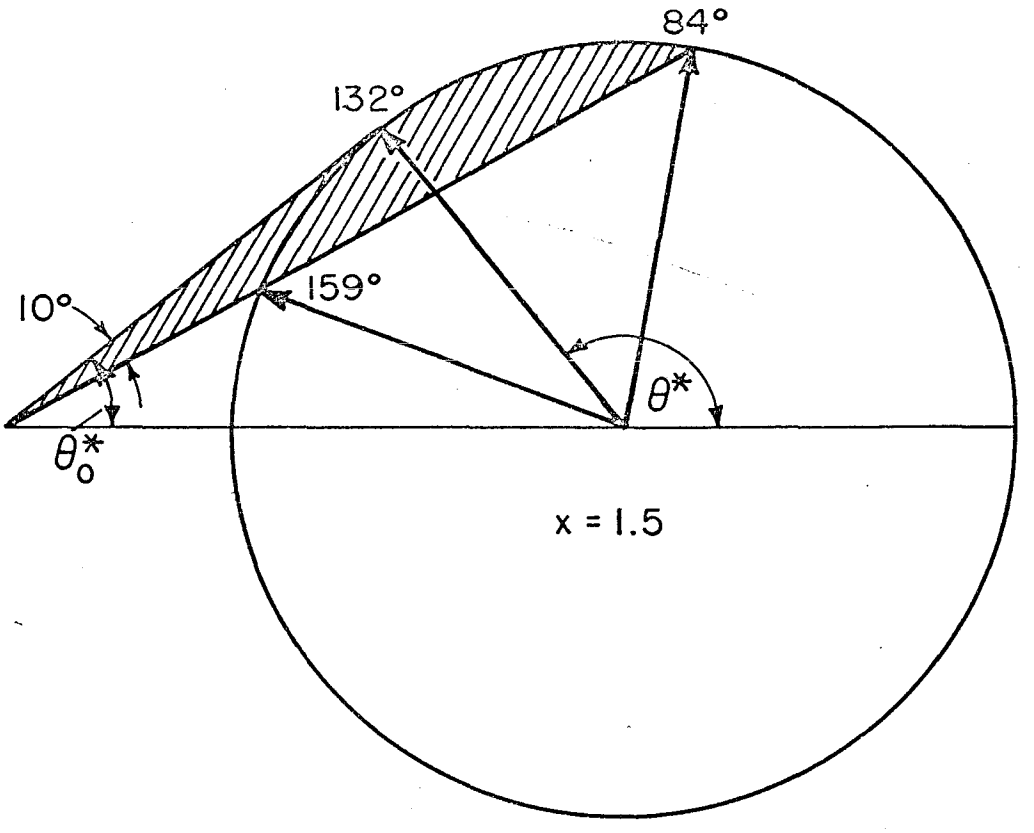

Fig. 9. Example of the "edge effect". For x = 1.5, the angular distribution between 84° and 159° in the center of mass system is compressed into a range of only 10° in the laboratory system.

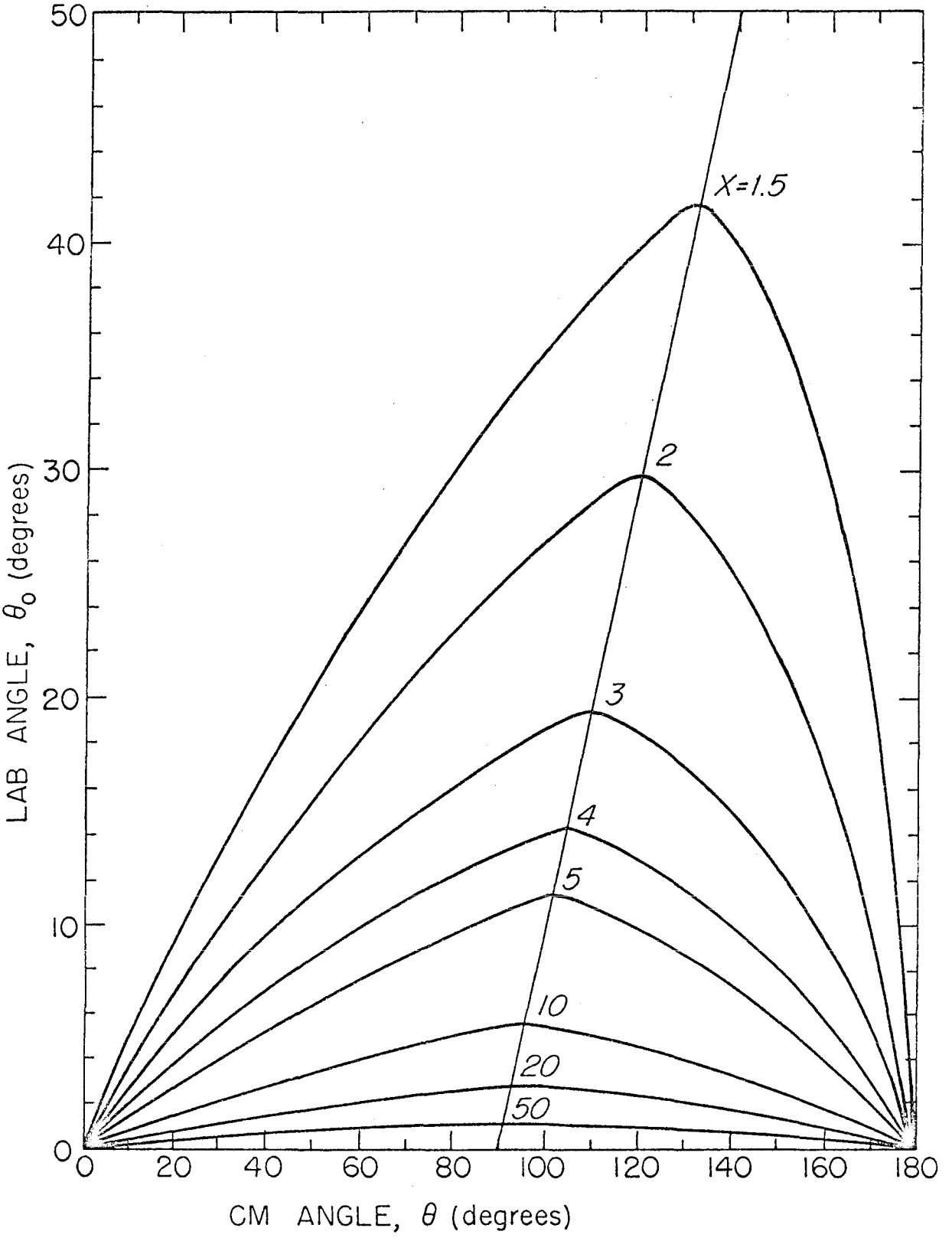

Fig. 10. Transformation between center of mass and laboratory angles for various values of the kinematic parameter x > 1, the case of "slow recoil".

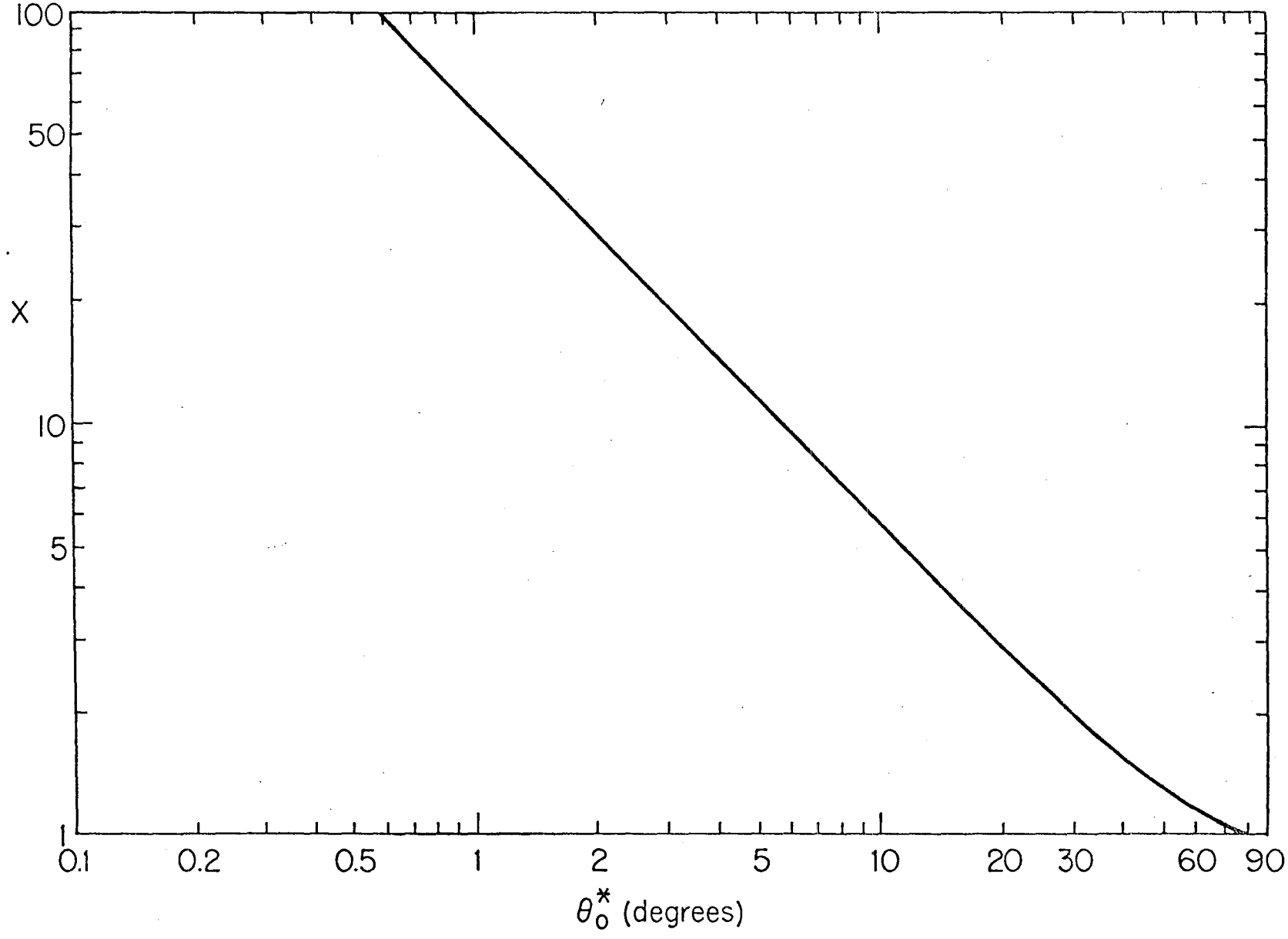

Fig. 11. Variation of the maximum laboratory scattering angle with the kinematic parameter x for case of "slow recoil".

the possible values of the kinematic parameter x, according to (17) and (18), and those portions of the CM recoil spectrum which lie near the singular sphere are heavily weighted in the LAB distribution. The edge angles are shown as functions of x in Figs. 10 and 11, which are from reference 6.

Figs. 4 and 5 illustrate how the laboratory angular distribution changes as the transition is made from "fast" to "slow" recoil. In Table V are given the angle of maximum laboratory intensity, θ_o (max), and the angle, θ_o (90°), which corresponds to the peak of the CM distribution at θ = 90°. The critical angles θ_o^* and θ^* are also shown as a function of x. The angle θ_o (max) is found from Eq. (21a) and θ_o (90°0 from Eq. (14). For $0 < x < 1$ we see that the angle at its maximum does not coincide with θ_o (90°) but is displaced from θ_o (90°) several degrees in the forward direction. This shift in the intensity maximum towards the beam direction, which is due to the Jacobian factor $J(x,\theta)$ in Eq. (21a) is noticeable even for $x < 1$ and is the precursor of the "edge effect". For x = 1, the CM distribution, proportional to $\sin^2\theta$, has a vanishingly small intensity near the critical angle θ^* and there is no singularity in the laboratory cross-section. The shape of the laboratory angular distribution still resembles the CM distribution although it is strongly skewed forward. For x = 1.25, the LAB distribution still reveals a large part of the lobe of the sine function before the edge singularity sets in. However, as x increases, this is soon swallowed up, and the LAB

Table V: Special angles in Figures 4 and 5

x	θ_o (90°)	θ_o (max)	θ_o^*	θ^*
0.00	90.0°	90.0°	. . .	. . .
0.25	76.0°	65.5°	. . .	. . .
0.50	63.4°	51.9°	. . .	. . .
0.75	53.1°	44.1°	. . .	. . .
1.00	45.0°	39.2°	90.0°	180.0°
1.25	38.7°	53.1°	53.1°	143.1°
1.50	33.7°	41.8°	41.8°	131.8°
1.75	29.8°	34.9°	34.9°	124.9°

distribution becomes practically a spike at the edge angle, $\theta_o = \theta_o^*$.

If only a single value of the kinematic parameter x were involved, the edge effect would enable a sharp measurement of x, and hence the partitioning of energy, to be obtained from the LAB angular distribution. However, there may be a considerable spread in values of x, corresponding to the velocity distribution in the molecular beam and the recoiling fragments. As illustrated later, this can produce a range of θ_o^* values much broader than the geometrical resolution and thereby drastically blur out the edge singularity.

Geometrical Resolution

In measuring the angular distribution in the laboratory, the differential angular distribution is never observed, but rather its average over the geometrical resolution of the apparatus:

$$I(\theta_o,\phi_o) = \frac{\int_{\phi_o-\Delta\phi_o}^{\phi_o+\Delta\phi_o}\int_{\theta_o-\Delta\theta_o}^{\theta_o+\Delta\theta_o} I(\theta,\phi)\sin\theta_o\, d\theta_o\, d\phi_o}{\int_{\phi_o-\Delta\phi_o}^{\phi_o+\Delta\phi_o}\int_{\theta_o-\Delta\theta_o}^{\theta_o+\Delta\theta_o}\sin\theta_o\, d\theta_o\, d\phi_o} \qquad (25)$$

For "fast" recoil the averaging over the geometrical resolution expressed by Eq. (25) very slightly smooths out the form of the angular distribution. For "slow" recoil the effect of this finite

angular resolution is to round off the edge singularity, leaving a spike or bump in the angular distribution where the singularity occurred. The magnitude of this spike will depend critically on the geometrical resolution of the apparatus and the velocity spread of the recoiling fragments.

In molecular beam scattering experiments the geometrical resolution is usually determined by the dimensions of the reaction zone rather than the width of the detector.[7,8] In a typical crossed-beam experiment[9] the area of the reaction zone is about 1 cm^2 and the detector is mounted about 10 cm away; thus the reaction zone subtends a solid angle of about 0.01 steradians at the detector. (By comparison, the area of a typical hot wire detector[9] is 0.005x1 cm^2, so at a distance of 10 cm it would subtend only 5×10^{-5} steradians at the scattering center.) For the initial attempts at beam studies of photodissociation of halogen compounds, a film detector which is chemically specific to halogen atoms appears to be a likely choice;[10,11] however, the area of the reaction zone will probably remain the limiting factor in determining the resolution.

To illustrate separately the blurring effect of imperfect geometrical resolution, we will evaluate Eq. (25) assuming that the velocities of the parent molecular beam and the recoiling fragment are fixed. We take $\Delta\theta_o$ and $\Delta\phi_o$ as constants, approximately equal to half of the angular height and width of the reaction zone, respectively. The calculation would be the same if the reaction zone were a point source

and the detector dimensions were $2\Delta\theta_o$ by $2\Delta\phi_o$; and our comments will refer to this case since it is simpler to describe. Thus, we regard the denominator of Eq. (25),

$$\Delta\Omega_o = 4\Delta\phi_o \sin\Delta\theta_o \sin\theta_o,$$

as the effective solid angle subtended by the detector at the reaction source. The numerator of Eq. (25) is most easily evaluated by transforming to the CM coordinate system. For the differential cross-sections $I(\theta,\phi)$ given in Table III, the integration can be performed analytically and the kinematic parameter x only enters via the limits of integration.

For "slow recoil" both the α and β branches contribute to the laboratory angular distribution. The limits of integration are given by

$$\phi_2 = \phi_o + \Delta\phi_o;\ \theta_2 = \theta_o + \Delta\theta_o \tag{26a}$$

$$\phi_1 = \phi_o - \Delta\phi_o;\ \theta_1 = \theta_o - \Delta\theta_o \tag{26b}$$

and

$$\left.\begin{matrix}\alpha_2\\ \beta_2\end{matrix}\right\} = \cos^{-1}\left[2x\cos\theta_2 \pm \frac{1 + x^2\cos 2\theta_2}{\sqrt{1 - x^2\sin^2\theta_2}}\right] \tag{27a}$$

$$\left.\begin{matrix}\alpha_1\\ \beta_1\end{matrix}\right\} = \cos^{-1}\left[2x\cos\theta_1 \pm \frac{1 + x^2\cos 2\theta_1}{\sqrt{1 - x^2\sin^2\theta_1}}\right]. \tag{27b}$$

In Eqs. (27) the plus sign refers to the angle α and the minus sign to the angle β. The averaged laboratory angular distribution

may now be wrttten as

$$I(\theta_o,\phi_o) = \frac{1}{\Delta\Omega_o}\left[\int_{\phi_1}^{\phi_2}\int_{\alpha_1}^{\alpha_2} I(\theta,\phi)\sin\theta d\theta d\phi - \int_{\phi_1}^{\phi_2}\int_{\beta_1}^{\beta_2} I(\theta,\phi)\sin\theta d\theta d\phi\right]$$

where the minus sign in Eq. (28) arises from the fact that $d\alpha = -d\beta$.

Eq. (28) is only valid provided that the leading edge of the detector, located at $\theta_o + \Delta\theta_o$, has not reached θ_o^*. When the leading edge reaches θ_o^*, that is, when the detector is centered at $\theta_o^* - \Delta\theta_o$, the intensity of the scattered particles attains its maximum. As the detector passes through the singularity, the leading portion of the detector moves outside the forward scattering cone and no particles can reach it. The limits of integration in Eq. (28) must then be changed appropriately by replacing α_2 and β_1 by θ^*. The value of Eq. (28) thus decreases as the detector moves past the singularity. When the trailing edge of the detector finally reaches the location of the singularity, α_1 and β_2 both become equal to θ^* and the integrals in Eq. (28) vanish.

An IBM 7090 computer program has been prepared which integrates the differential cross sections of type A, B, or C over the resolution widths and plots the resultant laboratory angular distributions. Fig. 12 illustrates the results for $\kappa = 1.25$ and 1.50 and a type B transition. Resolution widths between 1° - 4° should be feasible in

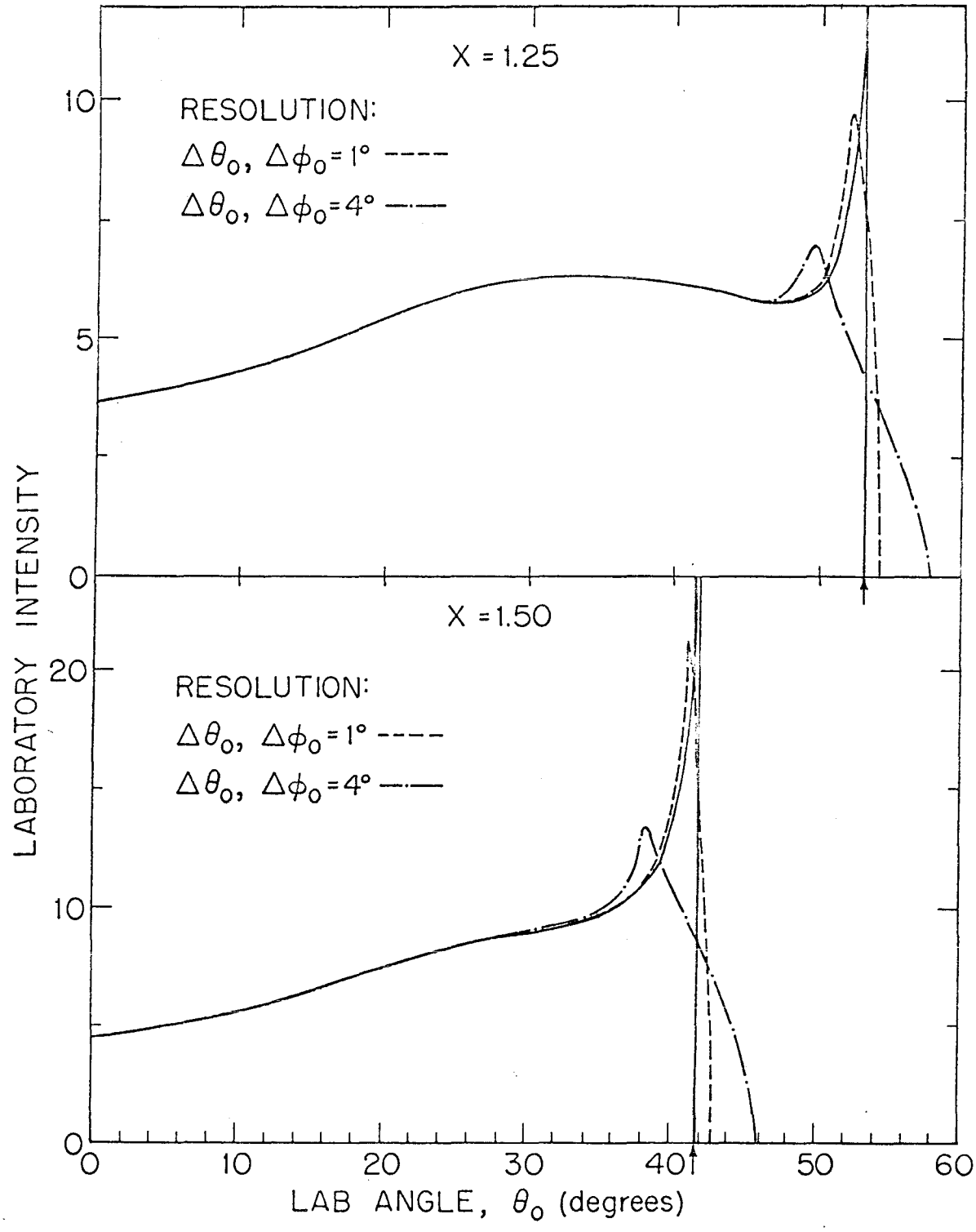

Fig. 12. Blurring of the "edge effect" due to finite angular resolution of the detector. The abscissa gives the location of the center of the detector. Arrows indicate location of the edge singularity in the differential cross section.

practice. The solid line gives the cross-section for infinite geometrical resolution. As could be anticipated from Figs. 4, 6, and 8, the larger the magnitude of x, the more pronounced is the spike. Although the finite angular resolution rounds off the singularity, if only one value of x were significant in an experiment, the resultant spike or bump would still be a prominent feature of the laboratory angular distribution of dissociation fragments.

Velocity Distribution of the Molecular Beam and Recoiling Fragments

The previous discussion has been restricted to fixed values of the molecular beam velocity V and the recoil velocity v_r and hence only one value of x. In practice, however, there will be a spread in x due to the velocity distribution in the parent molecular beam and the distribution in recoil velocities of the fragments. The latter distribution arises from the slope of the repulsive potential curve and the bandwidth of the exciting light beam. As mentioned before, this spread in x will cause further "blunting" of the edge singularity. Unless the intensity is sufficient to permit the luxury of velocity selection, which would reduce the signal about two orders of magnitude, this blurring will make the edge effect unobservable. We shall examine more closely the conditions necessary for its appearance.

For a highly monochromatic light source, such as an atomic line, the variation of x will be due primarily to the molecular beam velocity

distribution. The generalization of the previous results for this case is quite straightforward. We denote the normalized velocity distribution of the molecules in the oven by f(V) so that the probability of finding a molecule with its velocity between V and V + dV is given by f(V)dV. The velocity distribution of the beam emerging from the oven will be Vf(V), but the velocity distribution in the reaction zone will be again f(V), since the faster molecules spend less time in the reaction zone than the slower ones by the velocity factor V. To obtain the laboratory angular distribution, we must average Eq. (25) over the velocity distribution:

$$\overline{I(\theta_o,\phi_o)} = \frac{\int_0^\infty f(V) I(\theta_o,\phi_o) dV}{\int_0^\infty f(V) dV} \tag{29}$$

We shall assume a Maxwell-Boltzmann distribution given by

$$f(V)dV = \frac{4}{\sqrt{\pi}} y^2 e^{-y^2} dy \tag{30}$$

where $y = |V|/|\alpha|$ is the ratio of the beam velocity V to the most probable velocity α. It will be convenient to introduce the parameter x_α which is given by the ratio of the most probable velocity α to the recoil velocity v:

$$x_\alpha = |\alpha|/|v|.$$

Let us suppose the molecular beam is velocity-selected about the most probable velocity α. For "slow" recoil the laboratory distribution

will be peaked about θ_o^* corresponding to arcsin (1/x). There will still be an experimental spread in the beam velocity and thus in x. We define the parameter ε as the percentage variation of the beam velocity about α. Then the velocity-selected LAB distribution is obtained by modifying Eq. (29) to read

$$\overline{I(\theta_o,\phi_o)} = \frac{\int_{1-\varepsilon}^{1+\varepsilon} \overline{I(\theta_o,\phi_o)}\, y^2 e^{-y^2} dy}{\int_{1-\varepsilon}^{1+\varepsilon} y^2 e^{-y^2} dy} . \qquad (31)$$

Eq. (31) has been evaluated by a computer program for different values of ε. Fig. 13 shows the results for a type B transition and typical values of $\alpha = 1.8 \times 10^4$ cm/sec and $x_\alpha = 1.25$. As the velocity spread increases, the bump in the neighborhood of the singularity is rapidly smoothed out. A similar study for $x_\alpha = 1.50$ shows that the edge effect is more persistant, but disappears for $\varepsilon = \pm 10\%$. Consequently, even a rather small velocity spread about the nominal velocity removes the edge effect, even if the angular resolution of the experiment is sharp.

Even if it were feasible to velocity select the beam with $\varepsilon = \pm 2.5\%$, the light source must in general be highly monochromatic. For a molecule with closely spaced rotational levels (significantly populated at the molecular beam temperature) a spread in the energy E of the light will be reflected by a spread in the translational energy ΔE_T, and thus, via Eq. (3a), a spread in the recoil velocity,

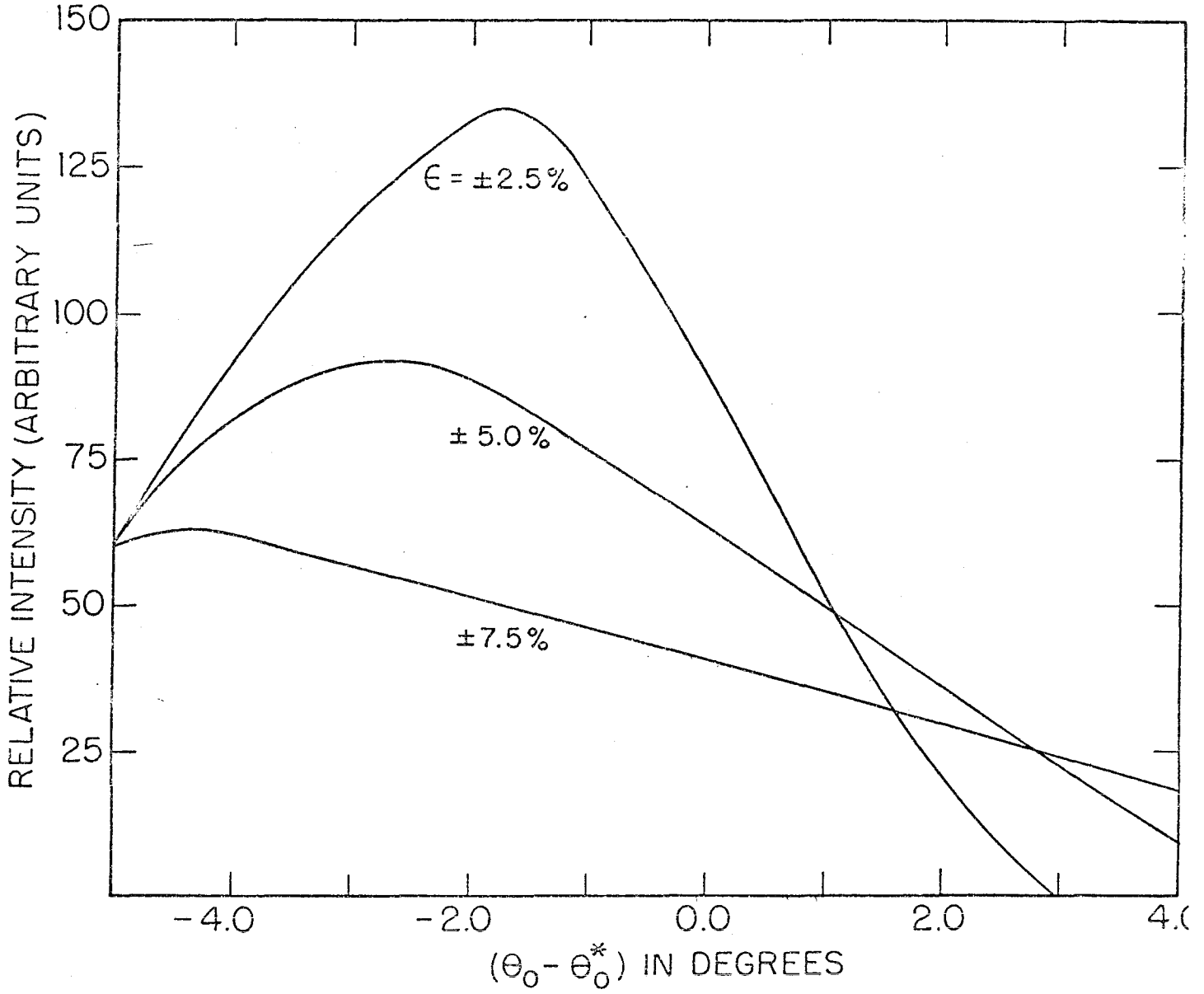

Fig. 13. Blurring of the "edge effect" in the neighborhood of the singular angle θ_o^* by the velocity spread in the parent molecular beam. The transition is of type B and the recoil parameter is $x_\alpha = 1.25$ for the most probable velocity in a beam of CH_3I at 300°K. The geometrical resolution is the 1° case of Fig. 12. The parameter ε gives the percentage range of velocity about the most probable velocity.

$$\Delta v_A = [(2m_B/mm_A)\Delta E_T]^{1/2}. \qquad (32)$$

For example, a 1 Å spread in the 2537 Å line (medium pressure mercury arc) corresponds to an energy uncertainty of 15.5 cm^{-1} in ΔE_T. If the observed fragment is about 10 times heavier than its fragment partner, by Eq. (31) there will be a spread in the recoil velocity of about 1.8×10^3 cm/sec. For an average α of 1.8×10^4 cm/sec this is comparable to $\varepsilon = \pm 10\%$, and the edge effect would be washed out. In fact, under beam conditions one will probably have to work with a rather broad pumping source to produce a sufficient number of photodissociation fragments for detection. Thus these calculations demonstrate that in practice the edge effect will be unobservable.

Fortunately, the "slow recoil" case which we have been considering up to now is only likely to obtain for photodissociation near the threshold.[1] Irradiation at energies appreciably above the threshold will usually produce "fast recoil" fragments, with velocity well above that of the parent beam. For this case, the velocity averaged angular distribution usually bears a close resemblance to that for the most probable kinematic parameter, x_α. This was confirmed by evaluating Eq. (29) with the full Maxwell-Boltzmann distribution for various values of $x_\alpha < 1$; the results for $I(\theta_o,\phi_o)$ were quite similar to $\overline{I(\theta_o,\phi_o)}$ for the fixed velocity $V = \alpha$, but were somewhat broader and were shifted a few degrees in the forward direction. Thus, for cases with $x_\alpha < 1$, the partitioning of energy in photodissociation can be determined without recourse to velocity selection.

The Photolysis of Methyl Iodide

The two major problems associated with measuring the energy partition in the photodissociation of a beam of polyatomic molecules are those of dissociating a reasonable number of molecules per second with radiation of well-defined energy and of finding a method of detecting one of the scattered fragments. These problems are of course related in that the smaller the rate of dissociation of the molecules in the beam, the greater the sensitivity requirements of the detector. We have made some simple order of magnitude calculations to determine what combination of detector and light source is necessary to measure the energy partition under beam conditions.

We shall limit ourselves to considering the photolysis of methyl iodide, although many of the estimates are applicable to other molecular systems. Methyl iodide is chosen for study as a prototype case since its photochemistry is relatively well-known and it has often been used as a source of "hot" methyl radicals.[12]

When methyl iodide absorbs radiation in the region of its ultraviolet continuum the molecule undergoes a primary dissociation, yielding predominangly methyl radicals in the ground electronic state and iodine atoms in the first excited state:

$$CH_3I \xrightarrow{h\nu} CH_3 + I(^2P_{1/2}).$$

This process requires 76 kcal/mole (54 kcal/mole to rupture the C—I bond and 22 kcal/mole to excite the iodine atom) corresponding to

3800 Å, so that excess energy will be available when CH_3I is dissociated at wavelengths below 3800 Å. For example at 2537 Å, near the maximum of the methyl iodide continuum,[13] 36 kcal/mole of excess energy will be distributed between the two dissociation fragments. If all of the excess energy were to appear as translational energy, the lighter methyl radical would carry away 32 kcal/mole and the heavier iodine atom 4 kcal/mole to conserve linear momentum. On the other hand, all the excess energy may be found in the internal degrees of freedom of the methyl radical. Thus the "hot" methyl radical in either case must carry away at least 32 kcal/mole of the excess energy.

It has been shown by Mulliken[14] and recently by Herzberg[15] that absorption by CH_3I of the intense 2537 Å Hg line corresponds to a perpendicular transition from the ground state $^1\Sigma^+$ ($^1A_1$) to one of the components of the excited repulsive state $^3\Pi$ (^3E). For a beam of unpolarized light a type B transition would result, for which we have worked out several examples. If the photodissociation products separate with more than a few kcal/mole of translational energy, as might be expected above the dissociation threshold, then the detection of the heavier fragment (iodine atom) is preferable since its angular distribution is more strongly affected by the degree of energy partitioning.[9]

If we can assume Beer's law behavior

$$\sigma = \frac{1}{nd} \log \frac{I_o}{I} , \qquad (33)$$

it is simple to calculate the number of iodine atoms that might reasonably be expected in dissociating a beam of methyl iodide. In Eq. (33) n is the number of molecules/cc, d is the thickness of the absorbing gas in cm and I_o and I are the intensity of the incident and transmitted light, respectively. At 2537 Å, the molar extinction coefficient[13] of methyl iodide is 300 (moles/liter)$^{-1}$ cm^{-1}, corresponding to an absorption cross section of 4×10^{-18} cm^2. In order to meet the conditions for effusive flow, a molecular beam of CH_3I is limited to about 10^{13} molecules/cm^3. The dimensions of the reaction zone should be chosen to maximize the path length of the light. For 2537 Å radiation passing through a 1 cm x 1 cm x 0.5 cm reaction zone, Eq. (33) shows that the light will be attenuated to the extent of 5×10^{-6}. Thus the number of photons absorbed, which is equivalent to the number of molecules dissociated, is given by

$$I_o - I = 5 \times 10^{-6} I_o .$$

At 2537 Å, 1 watt of radiated power corresponds to 1.25×10^{18} photons/sec so that a 1 watt light source would produce 6×10^{12} iodine atoms/sec, and a 0.1 watt source, 6×10^{11} iodine atoms/sec. This may be compared to the successful crossed beam reaction[9]

$$K + CH_3I \rightarrow KI + CH_3 .$$

Under very similar conditions, only 1×10^{11} molecules/sec of KI fly out of the reaction zone but this is sufficient for detection by surface ionization.

We shall review the available light sources and then examine

possible halogen atom detectors. Dr. R. M. Martin has studied this problem in detail and we shall summarize some of his findings.

Low pressure Mercury lamps using Vycor envelopes[16] could provide predominantly 2537 Å radiation at an intensity of 10^{16} - 10^{17} photons/sec in the reaction zone. All other sources require some form of filtering. Near ultraviolet absorbers[17] used in conjunction with a Vycor plate can isolate a band 400 Å wide (2600 - 2200 Å) and possibly a band 200 Å wide (i.e. 2500 - 2300 Å), but the peak transmission of such a filter would be of the order of 20 - 50% depending on the bandwidth. The major advantage of this type of filter over an interference filter is that the latter requires a collimated light beam. The maximum continuous intensity would be obtained with the Shannon 700/J light source[18] used with an absorption filter. If a filter with an average transmission of 10% in the 2500 - 2300 Å region were used, it is estimated that only 0.05 watts could be obtained in the reaction zone. Higher intensities could be achieved in principle by flashing compact arc Xenon-Mercury lamps.[19] An estimated 75 watts for 10^{-4} seconds might be achievable using an f/1 monochromater, but the construction of an apparatus with such a flash light source and monochromater would be a formidable task.

Either chemical or electronic detectors could be used with continuous photolysis, whereas flash photolysis would require an electronic detector with a short response time. T. A. Milne and P. W. Gilles[10] have used a tellurium film as a detector for fluorine atoms. The

film was about a monolayer thick, 4×10^{14} atoms/cm^2. If one needs to remove 10% of the film for development,[11] approximately 4×10^{13} iodine atoms/cm^2 must impinge upon the detector. If a minimum dissociation rate of 6×10^{11} molecules/sec were achieved and if 10^{-3} of these atoms struck a 1 cm^2 chemical detector, about 60 hours would be required for an experiment. Further investigation of this type of detector would be required to evaluate the performance of this detector in the presence of methyl radicals and excess methyl iodide.

The development of a surface ionization detector which would produce negative halogen ions is an attractive possibility because it would have short response time and would be specific for species with a high electron affinity. This requires a material with a suitably low work function. Kilpatrick[20] has suggested lanthanum hexaboride, LaB_6, which has a work function of 2.86 ev between 1000 - 1500°C. The electron affinity of iodine is about 3.2 ev so that the detector might be expected to produce negative iodine ions with close to 25% efficiency. However, at this temperature there would be considerable thermionic emission and a means must be provided for distinguishing between the negative ions and electrons.

Recently, universal molecular beam detectors employing electron bombardment ionization, ion multiplication, and mass spectroscopy have been developed[21,22] which can detect the order of 0.1 to 1% of a beam, at densities as low as 10^3 molecules/sec/cm^2, in a background of gas at 10^{-6} mm Hg. This beam density would correspond to a signal

of only about 2×10^{-14} amps for complete ionization of the beam. Provided that interfering signals could be reduced below this level by strong pumping and trapping, such a detector should permit beam studies of photodissociation.

From these order of magnitude estimates we conclude that beam studies of the photodissociation of polyatomic molecules which contain an alkali atom appear feasible. For these, we expect that conventional light sources and available surface ionization detectors would be adequate. However, the photochemistry of such compounds is poorly known. Beam studies of the photodissociation of other polyatomic molecules are probably also possible, but would demand a formidable investment in instrumentation.

Acknowledgment

We wish to thank Dr. R. M. Martin for carrying out a detailed examination of the feasibility of an experimental beam study of the methyl iodide photodissociation.

References

1. R. N. Zare and D. R. Herschbach, Proc. I.E.E.E. 51, 173 (1963).

2. R. N. Zare and D. R. Herschbach, University of California Radiation Laboratory Report UCRL-10438 (February, 1963).

3. H. Goldstein, Classical Mechanics (Addison-Wesley Publishing Co., Reading, Mass., 1951).

4. A. R. Edmonds, Angular Momentum in Quantum Mechanics (Princeton University Press, New Jersey, 1957).

5. For example, see L. I. Schiff, Quantum Mechanics (McGraw-Hill Book Co., Inc., New York, 1955), pp. 96 - 100; or L. D. Landau and E. M. Lifschitz, Classical Mechanics (Addison-Wesley Publishing Co., Inc., Reading, Mass., 1960), pp. 41 - 47. Useful tables have been prepared by J. B. Marion, T. I. Arnette, and H. C. Owens, Oak Ridge National Laboratory Report ORNL-2574 (April, 1959); however, it should be noted that Eq. (8) of this report is not valid for $x > 1$.

6. D. R. Herschbach, University of California Radiation Laboratory Report UCRL-9379 (April, 1960).

7. P. Kusch, "Notes on Resolution in Scattering Experiments" (Department of Physics, Columbia University, New York, 1960, unpublished).

8. R. G. J. Fraser, H. S. W. Massey, and C. B. O. Mohr, Zeit. f. Physik 97, 740 (1935).

9. D. R. Herschbach, Disc. Faraday Soc. 33, 149 (1962).

10. T. A. Milne and P. W. Gilles, J. Am. Chem. Soc., 81, 6115 (1959).

11. J. H. Simons and J. Glassner, J. Chem. Phys. 8, 547 (1940).

12. R. D. Schultz and H. A. Taylor, J. Chem. Phys. 18, 194 (1950).

13. D. Goodere and C. F. Porret, Proc. Roy. Soc. A165, 31 (1938).

14. R. S. Mulliken, J. Chem. Phys. 8, 382 (1940). See also R. S. Mulliken, Phys. Rev. 61, 277 (1942).

15. G. Herzberg, Disc. Faraday Soc. 35, 7 (1963).

16. Information on the Hanovia SC-2537 and other standard stock models is available from Engelhard Hanovia, Inc. Hanovia Lamp Division, Newark, New Jersey.

17. Possible chemical filters are Cl_2 [See H. van Halban and K. Siedentropf, Z. Physik Chem. 103, 71 (1922)] and an aqueous solution of I_2 and K [See W. A. Nozes, Jr. and P. A. Leighton, The Photochemistry of Gases p. 69, Reinhold Publishing Corp., New York, New York, (1941)

18. Shannon Luminous Materials Co., Los Angeles, California.

19. "Hanovia Compact Arc Lamps", Hanovia Lamp Division, Engelhard Hanovia, Inc., Newark, New Jersey.

20. W. Kilpatrick, "Experimental Investigations for Obtaining Stable Negative Ions" prepared for NASA Marshall Space Flight Center, Huntsville, Alabama. EOS Report 1981 - Final (December, 1961).

21. R. Weiss, Rev. Sci. Inst. 32, 397 (1961).

22. H. G. Bennewitz and R. Wedemeyer, Z. f. Phys. 172, 1 (1963).